CLOSED FORM OF THE STEERED ELONGATED HERMITE-GAUSS WAVELETS

Papari, Giuseppe; Campisi, Patrizio; Petkov, Nicolai

Published in:
2010 IEEE INTERNATIONAL CONFERENCE ON IMAGE PROCESSING

Publication date:
2010

CLOSED FORM OF THE STEERED ELONGATED HERMITE-GAUSS WAVELETS

Giuseppe Papari, Patrizio Campisi**, Nicolai Petkov**

* Johan Bernoulli Institute of Mathematics and Computing Science, University of Groningen
** Dipartimento di Elettronica Applicata, Universita' degli Studi Roma Tre, Roma, Italy

ABSTRACT

We provide a closed form, both in the spatial and in the frequency domain, of a family of wavelets which arise from steering elongated Hermite-Gauss filters. These wavelets have interesting mathematical properties, as they form new dyadic families of eigenfunctions of the 2D Fourier transform, and generalize the well known Laguerre-Gauss harmonics. A special notation introduced here greatly simplifies our proof and unifies the cases of even and odd orders. Applying these wavelets to edge detection increases the performance of about 12.5% with respect to standard methods, in terms of the Pratt's figure of merit, both for noisy and noise-free input images.

Index Terms— Edge features, Fourier analysis, Steerable filters

1. INTRODUCTION

The wavelet theory plays a central role in image processing [1]. An important complete family of orthogonal wavelets is given by the Hermite-Gauss filters (HGF) [2], which are very close to the optimal for feature detection [3] and have interesting causality properties for regularization in the scale-space [4, 5]. Moreover, these filters are *steerable* [6], i.e., their rotated versions with every angle can be expressed as linear combinations of fixed bases. This makes them suitable to detect oriented features. These wavelets find many image analysis applications, such as local features detection, texture modeling, and astronomical image compression, just to cite a few.

An intrinsic limit of HGF, pointed out by Canny [3], is that high noise rejection implies low localization accuracy and vice-versa. Such a limit is outrun by considering *elongated* filters (Fig. 1) which, however, are no longer steerable. A powerful framework to design steerable approximations of a given profile, which is widely applied in image processing, consists in expanding filters into series of orthogonal functions (single value decomposition [7, 8]). However, closed forms of the resulting bases are hardly available.

In this paper, we derive the closed form of an important family of filters that arise from steering elongated HGF, and we show some interesting mathematical properties of them. A special notation introduced here greatly simplifies our proof unifying the cases of even and odd orders of the Hermite functions. We also show experimental results related to the application of these wavelets to edge detection.

2. STEERING BASES OF THE ELONGATED HGF

In this section, we introduce the basis functions for steering the elongated HGF $H_{m,n}(x, y, \lambda)$. By definition, we have:

$$H^{\lambda}_{m,n}(x, y) \triangleq H_m(\lambda x) H_n(\lambda^{-1} y) e^{-\frac{(\lambda x)^2 + (\lambda^{-1} y)^2}{2}} \qquad (1)$$

G. Papari's research is funded by NWO

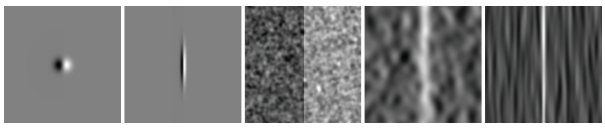

Fig. 1. From left to right: Non-elongated and elongated HGF of order (1,0), a noisy edge and its convolution with these two filters. Elongated filters have better localization for the same noise rejection.

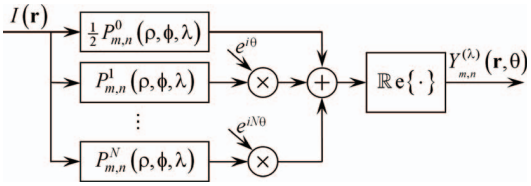

Fig. 2. Implementation of convolution with rotated elongated HGF.

where $\lambda > 0$ is a parameter and $H_n(x) \triangleq (-1)^n e^{x^2} \frac{\mathrm{d}^n}{\mathrm{d}x^n} e^{-x^2}$ is the n-th order Hermite polynomial. Let R_θ be the rotation matrix with angle θ. We wish to express $H^{\lambda}_{m,n}(R_\theta \mathbf{r})$ as a linear combination of fixed *steering bases* $P^s_{m,n}(\mathbf{r}, \lambda)$ with coefficients $a_s(\theta)$. It can be shown [6, 9] that such bases are the terms of the Fourier expansion of $H^{\lambda}_{m,n}(\rho\cos\phi, \rho\sin\phi)$ w.r.t. the angular coordinate ϕ, and that $a_s(\theta) = e^{is\theta}$. Moreover, $P^s_{m,n}(\mathbf{r}, \lambda)$ are circular harmonic functions (CHF), i.e., they are the product of a radial term $U^s_{m,n}(\rho, \lambda)$ with $e^{is\phi}$. Thus we have:

$$H^{\lambda}_{m,n}(R_\theta \mathbf{r}) = \sum_{s=-\infty}^{\infty} e^{is\theta} P^s_{m,n}(\mathbf{r}, \lambda) \qquad (2)$$

$$P^s_{m,n}(\rho, \phi, \lambda) = U^s_{m,n}(\rho, \lambda) e^{is\phi} \qquad (3)$$

Examples of the reconstruction of the filters $H^{\lambda}_{m,n}(R_\theta \mathbf{r})$ by means of the expansion (2) are shown in Figs. 3-4.

The convolution $Y^{\lambda}_{m,n}(\mathbf{r}, \theta) \triangleq I(\mathbf{r}) \star H^{\lambda}_{m,n}(R_\theta \mathbf{r})$ of an image $I(\mathbf{r})$ with a rotated elongated HGF is equal to:

$$Y^{\lambda}_{m,n}(\mathbf{r}, \theta) = \sum_{s=-\infty}^{\infty} e^{is\theta} [I(\mathbf{r}) \star P^s_{m,n}(\mathbf{r}, \lambda)]. \qquad (4)$$

By truncating (4) to the first N terms, the output $Y^{\lambda}_{m,n}(\mathbf{r}, \theta)$ can be computed for each θ by means of a few convolutions (Fig. 2).

3. CLOSED FORM OF THE STEERING BASES

In this section, we derive a closed form of the functions $U^s_{m,n}(\rho, \lambda)$ defined in (3). Let $\mathbf{U}_{m,n}(\rho; \lambda) \triangleq \{U^s_{m,n}(\rho; \lambda)\}^{\infty}_{s=-\infty}$ be a vector

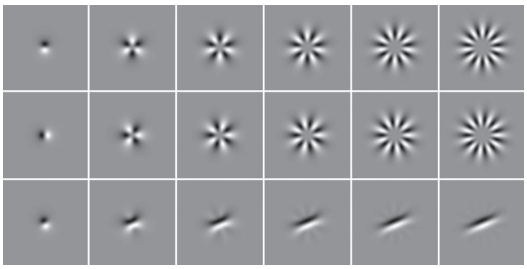

Fig. 3. (Top, middle), real and imaginary part of the first six non-zero steering bases $P^s_{0,1}(\mathbf{r},\lambda)$, for $\lambda = 2$. (Bottom) Reconstruction of rotated elongated HGF with the first N harmonics.

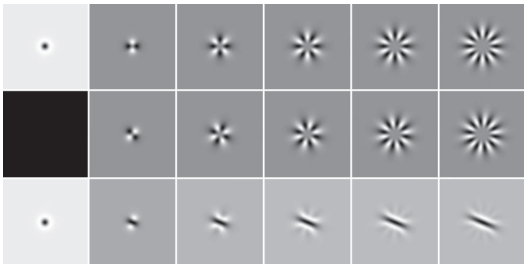

Fig. 4. Same as Fig. 3 for $(m,n) = (0,2)$.

whose components are the required bases. We need to evaluate the following integral:

$$\mathbf{U}_{m,n}(\rho;\lambda) = \frac{1}{2\pi}\int_0^{2\pi} H_m(\lambda\rho\cos\phi)H_n(\lambda^{-1}\rho\sin\phi)\times \\ \times\, e^{-\frac{(\lambda\rho\cos\phi)^2+(\lambda^{-1}\rho\sin\phi)^2}{2}} e^{-i\mathbf{k}\phi}\mathrm{d}\phi \quad (5)$$

with $\mathbf{k} \triangleq [...,-2,-1,0,1,2,...]^T$.

This integral can be simplified by means of basic properties of the Fourier coefficients, listed in Tab. 1 in a matrix form. Here, $\mathbf{x} \triangleq \{x_s\}_{s=-\infty}^{\infty}$ indicates the vector of the Fourier coefficients x_s of a periodic function $x(\phi) = \sum_s x_s e^{is\phi}$. Also, $\mathcal{S}$ indicates a *shifting matrix*[1] defined such that $\{\mathcal{S}\mathbf{a}\}_n = \{\mathbf{a}\}_{n+1}$ for every vector $\mathbf{a}$, where $\{\mathbf{a}\}_n$ denotes the n-th component of $\mathbf{a}$. Let also be:

$$\mathcal{R} \triangleq \frac{\mathcal{S}^{-1}+\mathcal{S}}{2}, \qquad \mathcal{I} \triangleq \frac{\mathcal{S}^{-1}-\mathcal{S}}{2i}. \quad (6)$$

These properties follow from the fact that a multiplication for $e^{is\phi}$ corresponds to a shift in the frequency domain. In particular, (P7-P9) are obtained from (P4-P5) due to the linearity of the Fourier operator. By using (P9) with $P(\cos\phi) = H_m(\lambda\rho\cos\phi)$ and $Q(\sin\phi) = H_n(\lambda^{-1}\rho\sin\phi)$, (5) rewrites as:

$$\mathbf{U}_{m,n}(\rho;\lambda) = H_m\left(\rho\lambda\mathcal{R}\right) H_n\left(\rho\lambda^{-1}\mathcal{I}\right)\times \\ \times\, \frac{1}{2\pi}\int_0^{2\pi} e^{-\frac{(\lambda\rho\cos\phi)^2+(\lambda^{-1}\rho\sin\phi)^2}{2}} e^{-i\mathbf{k}\phi}\mathrm{d}\phi \quad (7)$$

[1]The matrix $\mathcal{S}$ has an unlimited number of elements. In general, operations with infinite matrices are expressed in terms of infinite series, therefore convergence problems may occur. However, since the matrix $\mathcal{S}$ has only one nonzero element per row, convergence is trivially guaranteed. Convergence allows to manipulate unlimited matrices with the ordinary algebraic rules.

Table 1. Matrix form of the shifting properties of the Fourier coefficients, with P and Q polynomials

	Function	Coefficients vector
(P1)	$x(\phi)$	$\mathbf{x}$
(P2)	$x(\phi)e^{i\phi}$	$\mathcal{S}\mathbf{x}$
(P3)	$x(\phi)\cos\phi$	$\mathcal{R}\mathbf{x}$
(P4)	$x(\phi)\sin\phi$	$\mathcal{I}\mathbf{x}$
(P5)	$x(\phi)\cos^n\phi$	$\mathcal{R}^n\mathbf{x}$
(P6)	$x(\phi)\sin^n\phi$	$\mathcal{I}^n\mathbf{x}$
(P7)	$x(\phi)P(\cos\phi)$	$P(\mathcal{R})\mathbf{x}$
(P8)	$x(\phi)Q(\sin\phi)$	$Q(\mathcal{I})\mathbf{x}$
(P9)	$x(\phi)P(\cos\phi)Q(\sin\phi)$	$P(\mathcal{R})Q(\mathcal{I})\mathbf{x}$

Table 2. Analytical expression of the radial part $U^s_{m,n}(\rho;\lambda)$ of the steering bases of orders zero, one and two.

(m,n)	Functions $U^s_{m,n}(\rho,\lambda)$
(0,0)	$U^{2s}_{0,0}(\rho;\lambda) = e^{-\alpha\rho^2} I_s(\beta\rho^2)$ $U^{2s+1}_{0,0}(\rho;\lambda) = 0$
(1,0)	$U^{2s}_{1,0}(\rho;\lambda) = 0$ $U^{2s+1}_{1,0}(\rho;\lambda) = \frac{\lambda\rho}{2} e^{-\alpha\rho^2}[I_s(\beta\rho^2) + I_{s+1}(\beta\rho^2)]$
(0,1)	$U^{2s}_{0,1}(\rho;\lambda) = 0$ $U^{2s+1}_{0,1}(\rho;\lambda) = \frac{\lambda^{-1}\rho}{2i} e^{-\alpha\rho^2}[I_s(\beta\rho^2) - I_{s+1}(\beta\rho^2)]$
(2,0)	$U^{2s}_{2,0}(\rho;\lambda) =$ $e^{-\alpha\rho^2}\left\{\left(\frac{\lambda^2\rho^2}{2}-1\right) I_s(\beta\rho^2) + \frac{\lambda^2\rho^2}{4}[I_{s-1}(\beta\rho^2) + I_{s+1}(\beta\rho^2)]\right\}$ $U^{2s+1}_{2,0}(\rho;\lambda) = 0$
(1,1)	$U^{2s}_{1,1}(\rho;\lambda) = \frac{\rho^2}{4i} e^{-\alpha\rho^2}[I_{s-1}(\beta\rho^2) - I_{s+1}(\beta\rho^2)]$ $U^{2s+1}_{1,1}(\rho;\lambda) = 0$
(0,2)	$U^{2s}_{2,0}(\rho;\lambda) =$ $e^{-\alpha\rho^2}\left\{\left(\frac{\rho^2}{2\lambda^2}-1\right) I_s(\beta\rho^2) - \frac{\rho^2}{4\lambda^2}[I_{s-1}(\beta\rho^2) + I_{s+1}(\beta\rho^2)]\right\}$ $U^{2s+1}_{2,0}(\rho;\lambda) = 0$

This integral can be evaluated with basic calculus, by using the known result $\int_0^{2\pi} e^{x\cos u + isu}\mathrm{d}u = 2\pi I_s(x)$, where $I_s(x)$ is the s-th order modified Bessel function of the first type. The result is:

$$\frac{1}{2\pi}\int_0^{2\pi} e^{-\frac{(\lambda\rho\cos\phi)^2+(\lambda^{-1}\rho\sin\phi)^2}{2}} e^{-i\mathbf{k}\phi}\mathrm{d}\phi = e^{-\alpha\rho^2}\mathbf{I}\left(\beta\rho^2\right) \quad (8)$$

with:

$$\mathbf{I}(z) \triangleq [...,0,I_{-1}(z),0,I_0(z),0,I_1(z),0,...]^T, \quad (9)$$

and $\alpha \triangleq (\lambda^{-2}+\lambda^2)/4$, $\beta \triangleq (\lambda^{-2}-\lambda^2)/4$. Finally, combining (7) and (8), we obtain

$$\mathbf{U}_{m,n}(\rho;\lambda) = e^{-\alpha\rho^2} H_m\left(\lambda\rho\mathcal{R}\right) H_n\left(\lambda^{-1}\rho\mathcal{I}\right)\mathbf{I}\left(\beta\rho^2\right), \quad (10)$$

which is the required closed form.

In this expression, the term $H_m(\rho\lambda\mathcal{R})H_n(\rho\lambda^{-1}\mathcal{I})$ is a polynomial of the shifting matrices $\mathcal{S}$ and $\mathcal{S}^{-1}$ of degree $m+n$. Therefore, $U^s_{m,n}(\rho;\lambda)$ is the product of the Gaussian term $e^{-\alpha\rho^2}$ with a linear combination of modified Bessel functions of different orders, between $s-\left\lceil\frac{m+n}{2}\right\rceil$ and $s+\left\lceil\frac{m+n}{2}\right\rceil$, whose coefficients are expressed in terms of the Hermite coefficients and powers of $\lambda\rho$ and $\lambda^{-1}\rho$. Explicit expressions of the functions $U^s_{m,n}(\rho;\lambda)$ are given in Tab. 2 for the orders zero, one and two. As we see, the matrix form deployed in (10) considerably simplifies the notation and unifies the cases of even and odd indices (m,n).

4. SOME PROPERTIES OF THE STEERING BASES

In this section, we show some properties of the steering bases, which stem from the closed form (10).

1. *Conjugate symmetry*. We have $P^{-s}_{m,n}(\rho,\phi,\lambda) = \overline{P^{s}_{m,n}(\rho,\phi,\lambda)}$, where $\overline{z}$ indicates the complex conjugate of z.
2. *Zero terms*. We have $P^{s}_{m,n}(\rho,\phi,\lambda) = 0$ iff $m+n+s$ is an odd number. Properties 1 and 2 allow to reduce the computational complexity of expansion (4) by a factor four.
3. *Orthogonality*. As all CHF, the functions $P^{s}_{m,n}(\mathbf{r},\lambda)$ satisfy the orthogonality relation

$$\int P^{s}_{m,n}(\mathbf{r},\lambda)P^{p}_{m,n}(\mathbf{r},\lambda)\mathrm{d}^2\mathbf{r} = 0, \quad s \neq p, \tag{11}$$

   thus making, for any λ, multiple sets of orthogonal bases.
4. *Recursive formulas*. Using the well known identity $H_{n+1}(x) = xH_n(x) - H_{n-1}(x)$ into (10), we obtain the following recursive formulas for the steering bases:

$$P^{s}_{m+1,n}(\mathbf{r},\lambda) = \tfrac{\lambda\rho}{2}\left[P^{s-1}_{m,n}(\mathbf{r},\lambda) + P^{s+1}_{m,n}(\mathbf{r},\lambda)\right] - mP^{s}_{m,n}(\mathbf{r},\lambda)$$

$$P^{s}_{m,n+1}(\mathbf{r},\lambda) = \tfrac{\lambda^{-1}\rho}{2i}\left[P^{s-1}_{m,n}(\mathbf{r},\lambda) - P^{s+1}_{m,n}(\mathbf{r},\lambda)\right] - nP^{s}_{m,n}(\mathbf{r},\lambda)$$

   These formulas allow to recursively implement the steering bases of any order (m,n), which is faster than evaluating polynomials of matrices as in (10).
5. *Relation to Laguerre-Gauss harmonics*. Eq. (10) reduces to the Laguerre-Gauss harmonics for $\lambda = 1$. This can be demonstrated as follows. Let us consider the following expansion [2]:

$$H_m(x)H_n(y) = \sum_{s=-(m+n)}^{m+n} C^{s}_{m,n}\rho^{s}L^{|s|}_{\frac{m+n-s}{2}}(\rho^2)e^{is\phi} \tag{12}$$

   where $L^{n}_{\alpha}(x) \triangleq \frac{x^{-\alpha}e^{x}}{n!}\frac{\mathrm{d}^n}{\mathrm{d}x^n}\left(e^{-x}x^{n+\alpha}\right)$ are the generalized Laguerre polynomials, and $C^{s}_{m,n}$ is given by:

$$C^{s}_{m,n} = \left(\frac{m+n-s}{2}\right)!\sum_{r=0}^{m}(-1)^{r}\binom{m}{r}\binom{n}{\frac{m+n-s}{2}-r} \tag{13}$$

   when $m+n-s$ is even, and equal to 0 when $m+n-s$ is odd. By comparing expansions (2) and (12), we see that for $\lambda = 1$ and $s \leq m+n$ the steering bases reduce to

$$P^{s}_{m,n}(\rho,\phi,\lambda=1) = C^{s}_{m,n}e^{-\rho^2/2}\rho^{s}L^{|s|}_{\frac{m+n-s}{2}}(\rho^2)e^{is\phi} \tag{14}$$

   which are the well-known Laguerre-Gauss harmonics [10], while they reduce to 0 for $s > m+n$.
6. *Fourier transform*. Since the bases $P^{s}_{m,n}(\mathbf{r},\lambda)$ are CHF, their Fourier transform is a CHF as well, whose radial part is given by the s-th order Hankel transform of $U^{s}_{m,n}(\rho,\lambda)$ [10]. Its evaluation involves the solution of integrals in the form

$$\int_0^{\infty} x^{\alpha}e^{-\beta x}J_p(\gamma\sqrt{x})I_s(\delta x)\mathrm{d}x \tag{15}$$

   whose closed form is known [11]. A tedious computation yields the following interesting result:

$$P^{s}_{m,n}(\mathbf{r},\lambda) \xrightarrow{\mathcal{F}_{2D}} i^{m+n+s}P^{s}_{n,m}(\boldsymbol{\omega},\lambda). \tag{16}$$

   In other words, the 2D Fourier transform of a steering basis function is still a steering basis function. Moreover, for $m = n$ they make a dyadic family of eigenfunctions of the 2D Fourier transform, with eigenvalues i^{2n+s}.

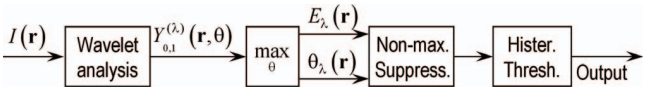

Fig. 5. Edge detection scheme.

5. EXPERIMENTAL RESULTS

We now show some experimental results related to the application of the steering bases to edge detection. We follow the approach depicted in Fig. 5, where the «Wavelet analysis» block is implemented through the filter bank detailed in Fig. 2. Our experiments show that the number of filters needed to achieve a neglectable reconstruction error is equal to λ^2. The filter bank output $Y^{\lambda}_{0,1}(\mathbf{r},\theta)$, defined in (4), detects edges oriented along the direction θ. Then, local edge direction $\theta_\lambda(\mathbf{r})$ and local edge strength $E_\lambda(\mathbf{r})$ are determined as

$$\theta_\lambda(\mathbf{r}) \triangleq \arg\max_{\theta} Y^{\lambda}_{0,1}(\mathbf{r},\theta), \qquad E_\lambda(\mathbf{r}) = Y^{\lambda}_{0,1}[\mathbf{r},\theta_\lambda(\mathbf{r})]. \tag{17}$$

An example of the edge strength $E_\lambda(\mathbf{r})$ is shown in Fig. 6 for $\lambda = 1$ and $\lambda = 2$, by keeping constant the product of the scale parameters across and along the edge direction. For high values of λ, edge localization is higher and contours are better preserved, such as in the elephant's tusks (marked by an arrow). Moreover, texture edges form structured chains of collinear edges, instead of meaningless random patterns. In Fig. 7, robustness to noise is shown. These results are related to the same smoothing orthogonally to the edge direction, which implies same edge localization. Larger values of λ allow for a larger smoothing along the edge direction, thus rejecting more noise. A larger set of examples is available on line[2].

Finally, edges are detected as in [3] by non-maxima suppression and thresholding. To quantify the performance of this approach, we compare the detected contours with hand drawn ground truths. Similarity between our results and ground truths has been measured in terms of the well-established Pratt's figure of merit F [12], which is always between 0 and 1, being 1 iff the detected contours coincide with the ground truth. The values of F, averaged over a set of 40 images, are plotted in Fig. 8 for different values of λ vs the fraction p of pixels above the threshold. As we see, higher values of λ result in an improvement of about 12.5% in terms of F. Further improvement could be achieved by deploying post-processing steps, similar to [13, 14].

6. SUMMARY AND CONCLUSIONS

We have shown that the wavelets resulting from steering the elongated HGF in the framework of single value decomposition [7] can be expressed analytically both in the spatial and the frequency domain. Specifically, the concerned functions are CHF, whose radial part is expressed in terms of a Gaussian term, modified Bessel functions of the first kind, and Hermite polynomials. Moreover, the matrix notation introduced here, considerably simplifies our derivation and unifies the cases of even and odd indices orders.

A closed form of the studied wavelets allows to carry out a deep theoretical study of their properties. In particular, we show that these filters make a new dyadic family of the 2D Fourier transform, thus making them interesting for some areas of signal and image processing, such as joint time-frequency analysis [15], as well as other areas

[2] http://www.cs.rug.nl/~imaging/ICIP2010

Fig. 6. From left to right: Input image and edge strength $E_\lambda(\mathbf{r})$ for λ = 1 and $\lambda = 2$, by keeping constant the product of the scale parameters across and along the edge direction.

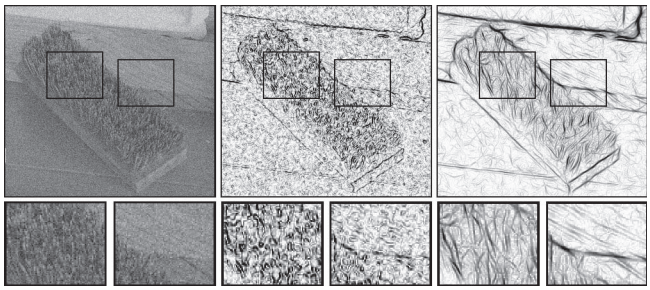

Fig. 7. First row, from left to right: noisy input image (SNR=13dB), edge strength $E_\lambda(\mathbf{r})$ for λ = 1 and $\lambda = 2$, and same amount of smoothing in the gradient direction. Second row: details.

of science, such as optics and quantum-mechanics. They also make a natural generalization of the well-known Laguerre-Gauss harmonics, which have successfully applied in many areas of image analysis, such as texture modeling, classification, stereoscopic imaging, denoising, and many others. Moreover, they can be implemented recursively, thus saving computation time.

The application of the steered elongated HGF of order $(m, n) = (0, 1)$ to edge detection allows to go beyond the Canny limit in the tradeoff between noise rejection and localization accuracy. In particular, while for 1D filters the maximum value of the Canny objective function is independent of scaling, in the 2D case it increases proportionally to $\lambda^2 = \sigma_y/\sigma_x$, where σ_x and σ_y are, respectively, the scale parameters in the direction orthogonal and parallel to the edge. Our experimental results are in agreement with this general principle. In particular, a performance increase of about 12.5% with respect to standard methods is achieved in terms of the Pratt's figure of merit.

7. REFERENCES

[1] S.G. Mallat et al., "A theory for multiresolution signal decomposition: The wavelet representation," *IEEE Trans. Patt. Anal. Mach. Intell.*, vol. 11, no. 7, pp. 674–693, 1989.

[2] I. Kimel and LR Elias, "Relations between Hermite and Laguerre gaussian modes," *IEEE Journal of Quantum Electronics*, vol. 29, no. 9, pp. 2562–2567, 1993.

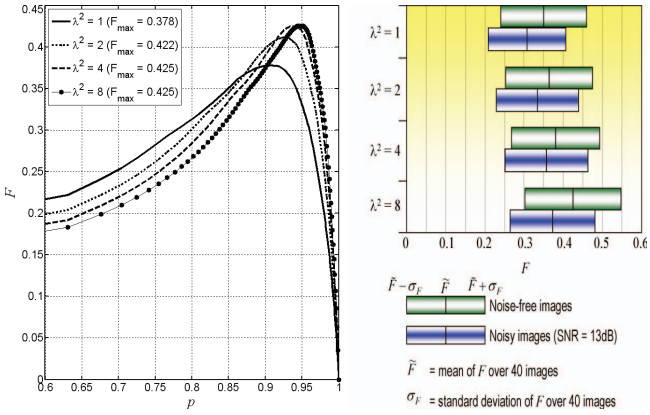

Fig. 8. Left: the average value of F a set of 40 noise-free images is plotted versus p. Right: mean and standard deviation of F, both for noise-free and noisy images, after optimization w.r.t p.

[3] J.F. Canny, "A computational approach to edge detection," *IEEE Trans. Patt. Anal. Mach. Intell.*, vol. 8, no. 6, pp. 679–698, 1986.

[4] A.L. Yuille and T.A. Poggio, "Scaling theorems for zero crossings," *IEEE T-PAMI*, vol. 8, no. 1, pp. 15–25, 1986.

[5] M. Bertero, T.A. Poggio, and V. Torre, "Ill-posed problems in early vision," *Proc. IEEE*, vol. 76, no. 8, pp. 869–889, 1988.

[6] W.T. Freeman and E.H. Adelson, "The design and use of steerable filters," *IEEE Trans. Patt. Anal. Mach. Intell.*, vol. 13, no. 9, pp. 891–906, 1991.

[7] P. Perona, "Deformable kernels for early vision," *IEEE Trans. Patt. Anal. Mach. Intell.*, vol. 17, no. 5, pp. 488–499, 1995.

[8] P.C. Teo and Y. Hel-Or, "Design of multiparameter steerable functions using cascade basis reduction," *IEEE Trans. Patt. Anal. Mach. Intell.*, vol. 21, no. 6, pp. 552–556, 1999.

[9] P. Perona, "Steerable-scalable kernels for edge detection and junction analysis," *Image and Vision Computing*, vol. 10, no. 10, pp. 663–672, 1992.

[10] G. Jacovitti and A. Neri, "Multiresolution circular harmonic decomposition," *IEEE Transactions on Signal Processing*, vol. 48, no. 11, pp. 3242–3247, 2000.

[11] O.I. Marichev A.P. Prudnikov, Yu.A.Brychkov, *Integrals and Series. Volume 2: special functions*, Gordon and Breah Science Publisher, 1992.

[12] I.E. Abdou and W.K. Pratt, "Quantitative design and evaluation of enhancement/thresholding edge detectors," *Proc. IEEE*, vol. 67, no. 5, pp. 753–763, 1979.

[13] G. Papari, P. Campisi, N. Petkov, and A. Neri, "A biologically motivated multiresolution approach to contour detection," *EURASIP J. Adv. Sign. Proc.*, vol. 2007, pp. Article ID 71828, 28 pages, 2007.

[14] G. Papari and N. Petkov, "Adaptive pseudo dilation for gestalt edge grouping and contour detection," *IEEE Transactions on Image Processing*, vol. 17, no. 10, pp. 1950–1962, 2008.

[15] L. Cohen, *Time-Frequency Analysis: Theory and Applications*, Prentice Hall, 1995.